high imperfection. (In reflection topographs, imperfect regions will always produce stronger *integrated* reflections than perfect regions and will also do so in transmission topographs under low-absorption conditions.) The island B is assumed to be as perfect as C, but is slightly misoriented with respect to C. The topograph images sketched in (b)–(e) could represent either reflection topographs or transmission topographs from a specimen thin compared with the dimension CD in Fig. 2.7.1.2. [Possible distortion of the images relative to the shape of (a) is neglected: this matter is considered later.] First, suppose that continuous radiation is emitted from the source S. If the ratio b/a is quite small, the topograph image will resemble (b). The island A is detected by diffraction contrast whereas island B will not show any area contrast since by assumption the incident radiation contains wavelengths enabling B to satisfy the Bragg condition just as well as C. The low-angle B–C boundary may show up, however, since it contains dislocations that will produce diffraction contrast and might be individually resolvable with a high-resolution topographic technique. Orientation contrast of B becomes manifest when b is increased, and measurement of the misorientation is then possible from the displacement of the image of B [as shown in (c)] consequent upon the different direction of Bragg-reflected rays issuing from it compared with those from C.

Next, suppose that S emits a limited range of wavelengths, *e.g.* characteristic $K\alpha$ radiation, and let the incident beam be collimated to have an angular spread in the plane of incidence that is smaller than the component in that plane of the misorientation between B and C, but larger than the angular range of reflection of C or A. Then, if the specimen is rotated about the ω axis so that A and C satisfy the Bragg condition, B will not do so and the topograph will resemble (d). [Island A shows up in (d) by diffraction contrast, as in (b).]. Appropriate rotation of the specimen will bring B into the Bragg-reflecting orientation, but will eliminate reflection from A and C, as shown in (e). The images (d) and (e) will not undergo significant change with variation in the ratio b/a, except for loss of resolution as b/a increases. The sensitivity of misorientation measurement will increase as the angular and wavelength spread of the incident beam are reduced, but when the angular range of a monochromatic incident beam is lowered to a value comparable with the angular range of reflection of the perfect crystal (generally only a few seconds of arc), it will not be possible with one angular setting alone to obtain an image that will distinguish between diffraction contrast and orientation contrast in the clear way shown in (d). The distinction will require comparison of a series of topographs obtained during a step-wise sweep of the angular range of reflection by the specimen. This is the procedure adopted in double-crystal or multicrystal topography, as described in Sections 2.7.3 and Subsection 2.7.4.2.

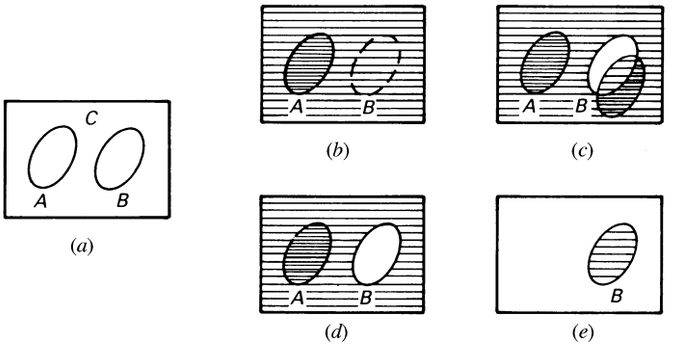

Fig. 2.7.1.3. Differentiation between orientation contrast and diffraction contrast in types of topograph images, (b)–(e), of a crystal surface (a).

Details concerning diverse variants in diffraction geometry used in X-ray topographic experiments, treatments of the diffraction contrast theory underlying X-ray topographic imaging of lattice defects, and listings of applications of X-ray topography can be found in reviews and monographs of which a selection follows. All aspects of X-ray topography are covered in the survey edited by Tanner & Bowen (1980). Armstrong & Wu (1973), Tanner (1976), and Lang (1978) describe experimental techniques and review their applications. The dynamical-diffraction theoretical basis of X-ray topography is emphasized by Authier (1970, 1977). Kato (1974) and Pinsker (1978) deal comprehensively with X-ray dynamical diffraction theory, which is also the topic of Part 5 of *IT* B (1996). Introductions to this theory have been presented by Batterman & Cole (1964), Hart (1971), and Hildebrandt (1982), the latter two being especially relevant to X-ray topography.

2.7.2. Single-crystal techniques

2.7.2.1. *Reflection topographs*

Combining the simple diffraction geometry of Fig. 2.7.1.1 with a laboratory microfocus source of continuous radiation offers a simple yet sensitive technique for mapping misorientation textures of large single crystals (Schulz, 1954). One laboratory X-ray source much used produces an apparent size of S 30 μm in the axial direction and 3 μm in the plane of incidence. Smaller source sizes can be achieved with X-ray tubes employing magnetic focusing of the electron beam. Then b/a ratios between $\frac{1}{2}$ and 1 can be adopted without serious loss of geometric resolution, and, with $a = 0.3$ m typically, misorientation angles of $10''$ can be measured on images of the type (c) in Fig. 2.7.1.3. The technique is most informative when the crystal is divided into well defined subgrains separated by low-angle boundaries, as is often the case with annealed melt-grown crystals. On the other hand, when continuous lattice curvature is present, as is usually the case in all but the simplest cases of plastic deformation, it is difficult to separate the relative contributions of orientation contrast and diffraction contrast on topographs taken by this method. In principle, the separation could be effected by recording a series of exposures with a wide range of values of b, and it becomes practicable to do so when exposures can be brief, as they can be with synchrotron-radiation sources (see Section 2.7.4.).

For easier separation of orientation contrast and diffraction contrast, and for quicker exposures with conventional X-ray sources, collimated characteristic radiation is used, as in the Berg–Barrett method. Barrett (1945) improved an arrangement earlier described by Berg (1931) by using fine-grain photographic emulsion and by minimizing the ratio b/a, and achieved high topographic resolution (∼ 1 μm). The method was further developed by Newkirk (1958, 1959). A typical Berg–Barrett arrangement is sketched in Fig. 2.7.2.1. Usually, the source S is

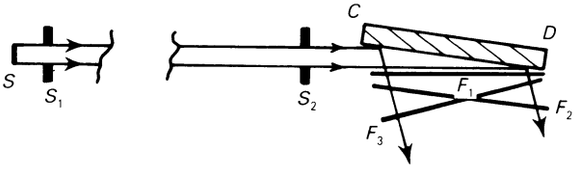

Fig. 2.7.2.1. Berg–Barrett arrangement for surface-reflection topographs.

references